LA-UR- 08-5617

Approved for public release; distribution is unlimited.

Title:	The importance of tilted rotation in nonhydrostatic ocean modelling
Author(s):	Nicole Jeffery and Beth A. Wingate
Intended for:	publication in the Journal of Physical Oceanography

Form 836 (7/06)

A linear stability analysis of the inviscid stratified Boussinesq equations is presented given a steady zonal flow with constant vertical shear in a tilted f-plane. Full nonhydrostatic terms are included: 1) acceleration of vertical velocity and 2) Coriolis terms arising from the meridional component of Earth's rotation vector. Calculations of growth rates, critical wavenumbers, and dominance regimes for baroclinic and symmetric instabilities are compared with results from the traditional nonhydrostatic equations, which include a strictly vertical rotation vector, as well as results from the hydrostatic equations. We find that tilted rotation enhances the dominance regime of symmetric instabilities at the expense of baroclinic instabilities and maintains symmetric instabilities to larger scales than previously indicated. Furthermore, in contrast to former studies, we determine that hydrostatic growth rates for both instabilities are not maximal. Rather, growth rates peak in the fully nonhydrostatic equations for parameter regimes physically relevant and consistent with oceanic measurements of the Labrador Sea and Southern Ocean. Results suggest that implementation of the fully nonhydrostatic equations should be considered for high-latitude numerical modelling.

---

1. Introduction

Of fundamental importance in geophysical fluid dynamics is the relation between balanced flows and vorticity production which has implications for understanding atmospheric storms or oceanic eddies. One of the simplest pictures of eddy production is the Eady (1949) model: a zonal flow with linear z-shear is maintained in steady balance with a meridional temperature gradient. This thermal wind balance provides a store of potential and kinetic energy to drive the production of eddies via rotational shear instabilities, most notably, the symmetric and baroclinic instabilities.

In the 1960's and 1970's, Stone published a series of papers in which he used linear stability analyzes to calculate and compare growth rates of two competing shear instabilities, symmetric and baroclinic (Stone 1966, 1970, 1971). He observed that the Richardson number (R_i, the square of the ratio of stratification to shear) determines an instability's dominance regime: the set of parameter values for which the instability's maximum growth rate exceeds that of all competing instabilities. For $R_i > 0.95$, Stone concluded that baroclinic instability, which converts base state potential energy to rolls of cross-wise vorticity, has maximal rates. However, for $0.25 < R_i < 0.95$, the symmetric instability dominates, and base state kinetic energy, primarily, feeds the production of stream-wise vorticity rolls. The R_i criteria proved valid for both hydrostatic and traditional nonhydrostatic models, though instability growth rates were found to depend upon the vertical velocity acceleration term (Dw/Dt) particularly for the symmetric instability.

Although Stone (1971) first suggests that nonhydrostatic effects may be important for resolving symmetric instabilities, his nonhydrostatic model employs the traditional approximation, i.e. Coriolis terms containing the meridional component of the Earth's rotation vector are neglected. Hathaway et al. (1979), Sun (1994) and Mu et al. (1998) go beyond the traditional approximation to include both components of the tilted rotation vector in their studies of the nonhydrostatic symmetric instability and find that nonhydrostatic parameters alter the R_i criteria. However, their work assumes a hydrostatic base state which couples the static stratification to the vertical Coriolis term in the base state buoyancy field, rendering each contribution indistinguishable in the model parameter space.

In this work, we return to linear stability theory and Stone (1971)'s framework but include full components of the Coriolis force in our analysis of nonhydrostatic insta-

bilities. Our work extends the results of Hathaway et al. (1979), Sun (1994) and Mu et al. (1998) with the following important differences: 1) our base state decouples the static stratification from the vertical Coriolis terms enabling a greater exploration of the model parameter space, and 2) impacts to both symmetric and baroclinic instabilities are assessed. We find that nonhydrostatic terms, Dw/Dt and the Coriolis terms due to oblique rotation, modify dominance regimes and alter growth rates for both types of instabilities. Consequently, nonhydrostatic symmetric instabilities may occur at larger scales than previously indicated by hydrostatic and traditional nonhydrostatic solutions.

Our primary interest is in the Earth's oceans and revealing possible implications that nonhydrostatic terms may have for modelling. We consider a physically relevant parameter regime defined by three locations in the Earth's seas: the Bay of Biscay, the Southern Ocean and the Labrador Sea. Of the dimensional parameters which characterize these bodies of water, stratification is found to be the most significant determinant in assessing the importance of tilted rotation and Dw/Dt in a particular region. We find that parameter values for which nonhydrostatic effects are maximal are consistent with stratifications typical of the Labrador Sea and the Southern Ocean, while the Bay of Biscay is, to good approximation, hydrostatic. In the Labrador Sea, growth rates for both instabilities are notably enhanced by nonhydrostatic effects. Results indicate that the high-latitudes are the oceanic regions most sensitive to full nonhydrostatic terms.

Finally, we use our perturbation solutions to calculate kinetic and potential mean to eddy conversion rates and, then, estimate mean and eddy energy production rates for baroclinic and symmetric instabilities. The purpose of these estimates is to understand the extent to which relative mean kinetic to potential energy loss rates become region-specific when tilted rotation and Dw/Dt are included. This dependence is most prominent for the symmetric instability.

2. Equations

We use the following notation in this work: fluid velocity, $\mathbf{u} = (u, v, w)$, represents zonal x, meridional y, and vertical z components, respectively; $\theta = p/\rho_o$ is pressure normalized by a constant reference density; and the Earth's rotation vector at a reference latitude ϕ_o includes both meridional and vertical components $\mathbf{\Omega} = (0, \Omega\cos\phi_o, \Omega\sin\phi_o) \equiv (0, F, f)/2$. We are interested in oceans with stable static stratifications and potentially destabilizing flow. The square of the Brunt-Väisälä frequency, $N^2 = -g/\rho_o d\rho_s(z)/dz > 0$, is proportional to gradients of the resting state density $\rho_s(z)$, and is taken to be constant, while the buoyancy, $b = -g[\rho - \rho_s(z)]/\rho_o$, is proportional to density deviations from the resting state and gravitational acceleration g.

Our analysis begins with the 3D inviscid and incompressible Boussinesq equations on a tilted f-plane:

$$\begin{aligned} \frac{D\mathbf{u}}{Dt} + 2\mathbf{\Omega}\times\mathbf{u} + \boldsymbol{\nabla}\theta - b\hat{\mathbf{k}} &= 0 \\ \frac{Db}{Dt} + wN^2 &= 0 \\ \boldsymbol{\nabla}\cdot\mathbf{u} &= 0 \end{aligned} \tag{2.1}$$

where $D/Dt \equiv \partial/\partial t + \mathbf{u}\cdot\boldsymbol{\nabla}$. To facilitate comparison with Stone (1971), we adopt his scaling in (2.1): $(x, y) = (\tilde{x}, \tilde{y})U_o/f$, $z = \tilde{z}D$, $t = \tilde{t}/f$, $(u, v) = (\tilde{u}, \tilde{v})U_o$, $w = \tilde{w}fD$, $\theta = \tilde{\theta}U_o^2$, and $b = \tilde{b}U_o^2/D$ where tildes denote non-dimensional variables, D is the vertical depth, and U_o the maximum background zonal velocity.

$$\begin{aligned} \frac{D\tilde{u}}{D\tilde{t}} + R_o^{-1}\cot\phi_o\tilde{w} - \tilde{v} + \frac{\partial\tilde{\theta}}{\partial\tilde{x}} &= 0 \\ \frac{D\tilde{v}}{D\tilde{t}} + \tilde{u} + \frac{\partial\tilde{\theta}}{\partial\tilde{y}} &= 0 \\ R_o^{-2}\frac{D\tilde{w}}{D\tilde{t}} - R_o^{-1}\cot\phi_o\tilde{u} + \frac{\partial\tilde{\theta}}{\partial\tilde{z}} - \tilde{b} &= 0 \end{aligned} \tag{2.2}$$

$$\frac{D\tilde{b}}{D\tilde{t}} + R_i\tilde{w} = 0 \tag{2.3}$$

$$\tilde{\boldsymbol{\nabla}} \cdot \tilde{\mathbf{u}} = 0 \tag{2.4}$$

It is convenient to define a modified normalized pressure $\theta^* = \tilde{\theta} - R_i\tilde{z}^2/2$ and buoyancy $b^* = \tilde{b} + R_i\tilde{z}$ which from (2.3) is a Lagrangian invariant $Db^*/D\tilde{t} = 0$. The solutions to the scaled equations depend on three non-dimensional numbers:

$$\begin{aligned} R_i &= \frac{N^2D^2}{U_o^2} \\ R_o &= \frac{U_o}{fD} = \delta_s^{-1} \\ \cot\phi_o &= \frac{F}{f} \end{aligned} \tag{2.5}$$

the Richardson number (R_i), the thermal Rossby number (R_o) or "baroclinicity" which is equivalent to the inverse of Stone (1971)'s aspect ratio (δ_s), and the ratio of tilted to vertical rotation (cotangent of the latitude). For the range of Richardson numbers investigated in this work ($R_i \in [0.25, 40]$), the relative importance of $D\tilde{w}/D\tilde{t}$ and tilted rotation terms diminishes with increasing baroclinicity. As $R_o \to \infty$, solutions converge to the hydrostatic limit.

In the remainder of this work, variables are assumed non-dimensional (unless otherwise stated) and represented without tildes and "modified" buoyancy and pressure are understood and represented without *. Subscripts of the independent variable will denote "differentiation by", for e.g. $u_t \equiv \partial u/\partial t$.

According to Sun (1994), stability properties and growth rates of the symmetric instability are not influenced by northward rotation effects when the base flow is meridional because the Coriolis contribution is trivially zero. A similar conclusion clearly follows for the baroclinic instability. Thus, in what follows, we restrict our analysis to strictly zonal base flows.

Consider a zonal base flow $U(z,y)$, modified buoyancy $B(y,z)$ and pressure $\Theta(y,z)$ in a horizontal plane of infinite extent bounded vertically by a flat bottom at $z=0$ and rigid lid at $z=1$. By (2.2)-(2.4), base state variables satisfy the relations:

$$U+\Theta_y=0 \quad \text{and} \quad -R_o^{-1}\cot\phi_o U+\Theta_z-B=0 \tag{2.6}$$

from which we conclude

$$B_y=-\left[R_o^{-1}\cot\phi_o U_y+U_z\right] \tag{2.7}$$

$$B_z=-\int U_{zz}dy'-R_o^{-1}\cot\phi_o U_z+\mathcal{B}_z(z) \tag{2.8}$$

where $\mathcal{B}_z$ is an arbitrary function of z representative of the static ocean stability and may be equated to the square of the Brunt-Väisälä frequency, i.e. $\mathcal{B}=R_i z$. There are two important points to note concerning the base state. First, from (2.7), meridional gradients in the vertical Coriolis force modify the thermal wind relation. Although latitude is fixed in this model, meridional gradients are possible in the base velocity and, certainly, more realistic. This additional complication will be the topic of future work and is not addressed here. The second point arises from (2.8). In general, base flow will modify the constant N^2 resting stratification via z-gradients in the zonal velocity and the meridional component of the rotation vector. In the case of a zonal flow linear in z, $B=R_i z-U_z y-R_o^{-1}\cot\phi_o U$. The several authors who have looked at this problem (Hathaway et al. (1979), Sun (1994) in (21a), Straneo et al. (2000) in (3), Mu et al. (1998)), combine the static stratification and the vertical Coriolis into a single linear function of z parameterized by a "base" Brunt-Väisälä frequency, i.e. $B=R_i' z-U_z y$ which also satisfies the thermal wind equation. We use the former result derived from (2.8) with $\mathcal{B}=R_i z$ which is more general, does not enforce a hydrostatic balance in the

base flow, and also applies to the more realistic case of meridionally confined or dependent zonal vertical shear. As well, by decoupling the static stratification (R_i dependent) from the vertical Coriolis (R_o and $\cot\phi_o$ dependent), we can explore stability properties in a more complete parameter space.

We are interested in disturbances about a base flow which may lead to rotational shear instabilities. We adopt Eady (1949)'s model of baroclinically unstable flow, $U = z$, which is the simplest example and was a starting point in the works of Stone and others (Hathaway et al. (1979), Sun (1994), Mu et al. (1998)). Let $u = U + u'$, $(v, w) = (v', w')$, $b = B + b'$ and $\theta = \Theta + \theta'$ where perturbation variables (assumed small) are denoted with primes. Retaining only linear terms, (2.2)–(2.4) become

$$\begin{aligned} u'_t + zu'_x + w'[1 + R_o^{-1}\cot\phi_o] - v' + \theta'_x &= 0 \\ v'_t + zv'_x + u' + \theta'_y &= 0 \\ R_o^{-2}\left[w'_t + zw'_x\right] - R_o^{-1}\cot\phi_o u' + \theta'_z - b' &= 0 \\ b'_t + zb'_x + v'B_y + w'B_z &= 0 \\ \boldsymbol{\nabla}\cdot\mathbf{u}' &= 0 \end{aligned} \tag{2.9}$$

Imposing a solution ansatz:

$$(u, v', w', \theta', b') \propto \mathrm{Re}\{(\hat{u}(z), i\hat{v}(z), i\hat{w}(z), \hat{\theta}(z), \hat{b}(z))\exp\{i(\sigma_o t + kx + \lambda y)\}$$

and letting $\sigma(z) = \sigma_o + zk$, (2.9) can be combined into a single, second-order, ordinary differential equation for vertical velocity

$$\begin{aligned} 0 = \left(1-\sigma^2\right)\hat{w}_{zz} + \left[2i\lambda(1 + R_o^{-1}\cot\phi_o) - \frac{2k}{\sigma}\right]\hat{w}_z - \left[k^2(R_i - R_o^{-1}\cot\phi_o) + \right. \\ \left. \lambda^2(R_i + R_o^{-2}\cot^2\phi_o) - R_o^{-2}(k^2+\lambda^2)\sigma^2 + \frac{2ik\lambda}{\sigma}(1 + R_o^{-1}\cot\phi_o)\right]\hat{w} \end{aligned} \tag{2.10}$$

subject to the boundary conditions: 1) $\hat{w}(z) = 0$ at $z = 0$ and 1 and 2) $\mathrm{Im}(\lambda) = \mathrm{Im}(k) = 0$ as required for finite solutions in an infinite horizontal domain. (2.10) reduces to Stone (1971)'s equation (2.25) with $\cot\phi_o = 0$ and further reduces to Eady (1949)'s equation (II) when $R_o \to \infty$. Note, the equivalent expression with B_z independent of U_z derived in Hathaway et al. (1979) eqn. 15) is missing the term $2k\hat{w}_z/\sigma$.

2.1. *Near the Symmetric Axis:* $k \to 0$

Several authors (Hathaway et al. (1979), Sun (1994), and Mu et al. (1998)) have studied the effects of a rotation axis tilted with respect to the vertical in connection with the symmetric instability. Most notably Hathaway et al. (1979) and Sun (1994) present results from a linear stability analysis given zonal base flow with constant vertical shear and full non-hydrostatic effects in the perturbation variables, however base vertical buoyancy gradients are restricted to be hydrostatic, $B_z = R_i$. By relaxing this condition, we are free to use the model non-dimensional parameter space to establish hydrostatic regimes and clarify the connection between the baroclinicity and the effects of tilted rotation.

Stone (1966) and (1971) established that symmetric instabilities occur for $\sigma_o \sim 1$ as $k \to 0$. In this limit (2.10) reduces to

$$0 = \left(1 - \sigma_o^2\right)\hat{w}_{zz} + \frac{2i\lambda}{R_o}\left(R_o + \cot\phi_o\right)\hat{w}_z - \frac{\lambda^2}{R_o^2}\left[R_i R_o^2 + \cot^2\phi_o - \sigma_o^2\right]\hat{w} \quad (2.11)$$

with solution

$$\hat{w} = \exp\left\{\frac{-i\lambda(R_o + \cot\phi_o)z}{R_o(1-\sigma_o^2)}\right\}\sin(m\pi z) \quad \text{for} \quad m = 1,\ 2,\ 3, \ldots \quad (2.12)$$

Substituting (2.12) into (2.11) and defining $\lambda_m \equiv \lambda/(m\pi)$, σ_o satisfies

$$0 = \sigma_o^4(1 + \lambda_m^2 R_o^{-2}) - \sigma_o^2[2 + \lambda_m^2(R_i + R_o^{-2}\sin^{-2}\phi_o)] + 1 +$$

$$\lambda_m^2(R_i - 1 - 2R_o^{-1}\cot\phi_o) \tag{2.13}$$

i.e.

$$\sigma_o^2 = \frac{2 + \lambda_m^2(R_i + R_o^{-2}\sin^{-2}\phi_o)}{2(1+\lambda_m^2 R_o^{-2})}\{1 \pm \left[1 - \frac{4(1+\lambda_m^2 R_o^{-2})(1+\lambda_m^2[R_i - 1 - 2R_o^{-1}\cot\phi_o])}{(2+\lambda_m^2[R_i + R_o^{-2}\sin^{-2}\phi_o])^2}\right]^{1/2}\} \tag{2.14}$$

A necessary condition for instability may be found by noting that maximum growth rates occur for $\lambda_m \to \infty$.

$$\lim_{\lambda_m\to\infty}\sigma_o^2 = \frac{R_i R_o^2 + \sin^{-2}\phi_o}{2}\left\{1 - \left[1 - \frac{[R_i - 1 - 2R_o^{-1}\cot\phi_o]}{[R_i R_o + R_o^{-1}\sin^{-2}\phi_o]^2}\right]^{1/2}\right\} \tag{2.15}$$

which for $\sigma_o^2 < 0$ implies

$$R_i < 1 + \frac{2\cot\phi_o}{R_o} \tag{2.16}$$

This result reduces to Stone (1966)'s criteria $R_i < 1$ for purely vertical rotation, i.e. $\cot\phi_o = 0$. Sun (1994) finds a similar result for the unbounded domain based on the work of Ooyama (1965) and Hoskins (1978). His result may be converted into the criteria for instability: $R_i < 1 + \cot\phi_o/R_o$ which differs by the factor two. Both (2.16) and the instability criteria of Sun (1994) are equivalent to Hoskins (1978) condition of negative base state Ertel potential vorticity, q (in dimensional variables):

$$\begin{aligned} fq &= (2\boldsymbol{\Omega} + \boldsymbol{\nabla}\times U\hat{i})\cdot\boldsymbol{\nabla}B \\ &= (0, M_z, -M_y)\cdot\boldsymbol{\nabla}B \\ &= \left|\frac{\partial(M,B)}{\partial(z,y)}\right| < 0 \quad \text{for instability} \end{aligned} \tag{2.17}$$

where $M = U - fy + Fz$ is the absolute momentum. In this form, the discrepancies between Stone (1966), Sun (1994) and (2.16) are made clear. Relative to Stone (1966),

the vertical Coriolis decreases z-gradients in M and increases z-gradients in B, and both contributions decrease q. The base state as defined in Sun (1994) includes only the former contribution.

In the comparisons to follow, we use the term "model" to refer to (2.10) and its solutions in three parameter limits: 1) $R_o \to \infty$ defines the "hydrostatic model", 2) finite R_o and $\cot\phi_o = 0$ defines the "traditional nonhydrostatic model", and 3) finite R_o and $\cot\phi_o \neq 0$ defines the "fully nonhydrostatic model". Oceanic "numerical models" will be referred to as such to avoid confusion.

In figure 1, the unstable growth rates of (2.15)(thick lines) are compared with the traditional nonhydrostatic results ($Dw/Dt \neq 0$ but $\cot\phi_o = 0$) (thin lines) depicted in Stone (1971)'s fig. 2 and the hydrostatic approximation (thinnest lines in (b) only). We use Stone (1971)'s choice of R_i, 0.5, and sampling of R_o: 1) 70 (dotted), 2) 1 (dashed) and 3) 0.5 (dash-dotted), with one notable addition, the $R_o = 3$ example (solid lines). In the traditional approximation ($F = 0$), symmetric perturbations of the nonhydrostatic model, in regions of negative q, lead to instabilities which grow slower than that of the hydrostatic model. In fact, the smaller the baroclinicity, and, thus, the greater the relative importance of Dw/Dt, the smaller the growth rate. When the traditional approximation is not made, unstable growth rates initially increase with decreasing baroclinicity, i.e. the $R_o = 3$ example. Hence, for a given R_i, the hydrostatic rate is not maximal. Rather growth rates peak at an intermediate value of baroclinicity, $R_o \sim \mathcal{O}(1)$.

A second novel feature of the fully nonhydrostatic model is evident in figure 1. Stone (1971) observed that Dw/Dt has no effect on the largest wavelength at which the instability grows. However, when full Coriolis terms are included, symmetric growth rates ($\sigma_i = -\mathrm{Im}(\sigma)$) are positive to larger scales than predicted by the hydrostatic model. In figure 1(b), wavenumber λ which scales with R_o^{-1} has been converted to wavelength,

$L_\lambda/D = 2\pi R_o \lambda^{-1}$, normalized by vertical depth to elucidate the scale dependence. In all cases, as R_o decreases, symmetric instabilities become confined to smaller scales. This reduction in scale, however, is not as pronounced in the fully nonhydrostatic model and, for all baroclinicities compared, growth rates remain positive to maximum scales of $L_\lambda/D > 1$.

2.2. *Near the Baroclinic Axis:* $\lambda \to 0$

Sun (1994) finds that tilted rotation modifies linear perturbations about a zonal flow with constant z shear "if, and only if" perturbations are functions of y, and, hence, they do not impact pure baroclinic instabilities. Stone (1971), in his analysis of nonhydrostatic baroclinic instabilities, finds only weak effects (without tilted rotation). That is, Dw/Dt always decreases peak baroclinic growth rates and has no effect on stability criteria. However, we already have some indications that these conclusions change in the presence of tilted rotation and a nonhydrostatic base state. As was demonstrated in the previous section, the z-gradients of the vertical Coriolis modify the base stratification, the base Ertel potential vorticity (q), and, consequently, the symmetric stability criteria. Since peak symmetric growth rates are about a factor of five greater than baroclinic rates in regions of negative q, we can expect a modified regime in R_i/R_o parameter space for which baroclinic instabilities dominate. As well, Sun (1994) defined a base R_i' which does not decouple the static stratification (R_i) from the vertical Coriolis ($\propto R_o^{-1}$), a contribution which will modify even pure baroclinic instabilities.

Stone (1966) and (1971) established that maximum growth rates for baroclinic instabilities occur for $k \sim \mathcal{O}(1)$ and $\sigma_o = kc$ as $\lambda \to 0$. In the baroclinic plane, (2.10) becomes

$$0 = \left(1 - k^2(c+z)^2\right)\hat{w}_{zz} - \frac{2}{c+z}\hat{w}_z - \left[k^2\left(R_i - \frac{\cot\phi_o}{R_o}\right) - \frac{k^4(c+z)^2}{R_o^2}\right]\hat{w} \quad (2.18)$$

which reduces to Stone (1971)'s nonhydrostatic result (eqn. 3.2) with $\cot\phi_o = 0$. Although we solve this equation numerically using a collocation method and present the results in the figures of this work, it is illuminating to compare Stone (1971)'s approximate solution for unstable growth under nonhydrostatic conditions with the analogous expression including tilted rotation. Let $w = w_o + k^2 w_1 + \cdots$ and $c = c_o + k^2 c_1 + \cdots$ into (2.18) and retain the first two terms:

$$\sigma_i \approx \frac{1}{2\sqrt{3}} \left[k - \frac{2k^3}{15} \left(1 + R_i - R_o^{-1} \cot\phi_o + \frac{5R_o^{-2}k^2}{42} \right) \right] \tag{2.19}$$

where

$$c_o = -\frac{1}{2} \mp \frac{i}{2\sqrt{3}}$$
$$c_1 = \pm \frac{i}{15\sqrt{3}} \left(1 + R_i - R_o^{-1} \cot\phi_o + \frac{5R_o^{-2}k^2}{42} \right)$$

The signature of the nonhydrostatic base buoyancy profile appears in the $\mathcal{O}(k^3)$ term, i.e. $B_z = R_i - R_o^{-1} \cot\phi_o$, which reduces to R_i as in Stone (1971) without tilted rotation or R_i' for a base state as defined in Sun (1994). The important point here is that the "weak" nonhydrostatic effects Stone refers to are of $\mathcal{O}(k^5)$ and negative and always decrease growth rates, whereas R_o^{-1} is the same order in k as R_i and positive which decreases the stabilizing effect of the stratification and increases growth rates.

In figure 2, numerical solutions of $\sigma_i = -\mathrm{Im}(c)k$ (thick lines), where c is the eigenvalue of (2.18), are compared with the traditional nonhydrostatic growth rates (thin lines, also numerically derived) whose approximate solutions are plotted in Stone (1971)'s fig. 1. The hydrostatic results (thinnest lines in (b)) are plotted but converge with the $R_o = 70$ dotted line in (a). Again, the choice of $R_i = 2$ and R_o are Stone's: 1) $R_o = 70$ (dotted), 2) $R_o = 0.1$ (dashed), and 3) $R_o = 0.03$ (dash-dotted), though we have added $R_o = 1$ (solid). In the traditional approximation ($F = 0$), along-flow perturbations of

baroclinically unstable flows in the nonhydrostatic model grow slower than that of the hydrostatic model. As with the symmetric perturbations, the smaller the baroclinicity, and, thus, the greater the relative importance of Dw/Dt, the smaller the growth rate. When the traditional approximation is not made, unstable growth rates initially increase with decreasing baroclinicity and fixed R_i. This is particularly evident in the $R_o = 1$ and 0.1 curves. As in the symmetric result, for a given R_i, the *hydrostatic rate is not maximal.* In fact, growth rates appear to peak at similar values of baroclinicity, $R_o \sim \mathcal{O}(1)$. This is interesting since baroclinic growth rates are much less sensitive to R_o than symmetric rates.

In figure 2(b), growth rates are plotted against the zonal wavelength normalized by the vertical depth, L_k/D, in order to remove the R_o dependence of the zonal wavenumber, k, and clarify the scale dependence of maximum growth rates. In contrast to the symmetric instability, baroclinic growth is confined to large scales and maximum rates peak at clearly defined wavenumbers. In general, for all models, as the relative importance of Dw/Dt increases, zonal wavelengths of maximum growth move to smaller horizontal scales. Wavelengths derived from the nonhydrostatic solutions with tilted rotation follow very closely the traditional nonhydrostatic results and deviate from the hydrostatic limit only at very small baroclinicities: $R_o \sim \mathcal{O}(10^{-2})$, when nonhydrostatic growth rates become small.

3. Implications for the Ocean

The results of the previous section and, in particular, the comparisons with Stone (1971), indicate that tilted rotation coupled with acceleration of vertical velocity enhances growth rates of both instabilities and extends symmetric instabilities to larger scales for parameter values of $R_o \leqslant \mathcal{O}(1)$, $R_i \sim \mathcal{O}(1)$ and $\phi_o = 45^o$. We now consider the following

questions: 1) do these parameter values appropriately characterize the physical ocean? 2) Can we more fully explore the relevant physical parameter space?

Of the dimensional parameters which characterize the physical ocean, the Brunt-Väisälä frequency (N) and the latitude (ϕ_o) are the most influential in determining the importance of tilted rotation. And, as we shall see, of the two, N has the most significance.

We consider three oceanic regions for their ranging typical deep water stratifications: the Bay of Biscay (BB) at 44°–48°N, the Southern Ocean (SO) at $\geqslant$ 60°S, and the Labrador Sea (LS) at 55°–60°N. van Aken et al. (2007) measured mean Brunt-Väisälä frequencies in the slope region of the Bay of Biscay of $\sim 3.1 - 3.5 \times 10^{-3}\ s^{-1}$ and low gradient Richardson numbers well below 1. The Southern Ocean, according to Heywood et al. (2002) is generally weakly stratified, with low values of Brunt-Väisälä frequency $(5.4 \pm 0.2) \times 10^{-4}\ s^{-1}$, and the Labrador Sea region (60°N), according to Lasier (1980), is characterized by a deep weakly stratified region of $2.1 \times 10^{-4}\ s^{-1}$.

Figure 3 is a comparison of growth rates for the above three stratifications typical of LS ($\triangle$), SO (o), and BB ($\square$) at three latitudes: 30°, 45°, and 60° indicated by decreasing thickness. In the top two plots ((a) and (b)), tilted rotation effects are included along with Dw/Dt, while the bottom two ((c) and (d)) are from solutions of the traditional nonhydrostatic equations ($\cot\phi_o = 0$). The hydrostatic curves in (a)–(d) are indicated by + (visible in (b)) which overlap the growth rate curves for BB in (a), (c), and (d). Baroclinic instabilities ($R_i = 2$) are on the left and symmetric ($R_i = 0.5$) on the right. The baroclinic results are the more straight forward. For the full range of latitudes described, nonhydrostatic effects are most evident at the weakest stratifications (LS) where they modify peak growth rates between $\sim$ 7–16% of the hydrostatic rate. The high stratification of BB establishes the region as "hydrostatic" independent of latitude.

Simply put, for the baroclinic instability, changes in stratification account for greater variations in non-dimensional growth rates than occur for changes in latitude.

For the symmetric instability with tilted rotation (b), all three regions show at least modest deviations from the hydrostatic result (BB has a maximum deviation of $\sim 5\%$). In the regions of weak stratifications (LS and SO), tilted rotation and Dw/Dt can account for a 20-30% change in peak hydrostatic growth rate, though the latitude dependence is also significant. The tilted f-plane approximation limits our ability to fully explore the latitudinal dependence of these results, particularly near the equator where the β effect becomes important. However, we conclude that for $\phi_o \in [30^o, 60^o]$ weak static stratification is a very important indicator of a regions sensitivity to tilted rotation and w-acceleration and observe that weakly stratified regions tend to be high-latitude.

In the remainder of this work, we set $\phi_o = 60^o$ rather than 45^o, which is more appropriate for the weak N regions, LS and SO, and will provide a more accurate estimate of nonhydrostatic effects where they are more likely to occur.

Figure 4 is an analogue of the Stone figures (1 and 2) with physically relevant values of R_o (see figure caption) evaluated from $R_i = 2$ (baroclinic) and 0.5 (symmetric), $\phi_o = 60^o$, and N from LS (dash-dotted), SO (dashed) and BB (solid). The oceanic values of R_o: a) 1 (LS) to 20 (BB) for baroclinic instabilities, and b) 2 (LS) to 30 (BB) for symmetric instabilities, are subsets of the ranges plotted in figures 1 and 2 and continue to illustrate many of the important features of tilted rotation and Dw/Dt on growth rates and scale, though with less pronounced effect than observed at $\phi_o = 45^o$. That is, for both instabilities, hydrostatic growth rates for a given R_i are not maximal, and unstable growth rates initially increase as baroclinicity decreases from the hydrostatic limit. Most significantly, the regime $R_o \sim \mathcal{O}(1)$, for which enhancement of growth rates due to nonhydrostatic terms is most important, is physically relevant.

In figures 5 and 6, maximum growth rates are presented as solid contours in the space of R_o and R_i. Thick solid lines are from solutions of the fully nonhydrostatic equations, (2.10) and (2.18), while the thin lines are eigenvalues of the traditional nonhydrostatic equations ($\cot\phi_o = 0$). Since symmetric instabilities are bounded by a necessary condition of negative q, we have included lines of zero q: 1) the dotted line at $R_i = 1$ as stated in Stone (1966) and appropriate for the traditional nonhydrostatic solutions, 2) the thick dash-dotted line defined in (2.16), and, in figure 5 only, 3) the thin dash-dotted line of Sun (1994). Also included, as physical references, are three dashed lines of constant N representative of the sample locations: the Bay of Biscay (BB), Southern Ocean (SO) and Labrador Sea (LS).

Symmetric maximum growth rates exceed maximum baroclinic rates in regions of negative q except in a small neighborhood of the boundary. Stone (1966), for example, finds baroclinic rates dominate for $R_i > 0.95$ when rotation is strictly vertical. Tilted rotation increases this boundary by at least 5% for baroclinicities of < 20, and both SO and LS fall in this range. For LS, the negative q boundary nearly doubles, and baroclinic instabilities are not preferred until R_i reaches almost 2.

In the large R_o limit (at fixed f), both Stone (1971)'s results (thin lines) and the fully nonhydrostatic rates (thick lines) converge to the hydrostatic values and become independent of the baroclinicity. This hydrostatic limit also depends on R_i, i.e. convergence occurs for smaller values of R_o at larger R_i. Thus, with or without tilted rotation, baroclinic instabilities are hydrostatic for a greater range of stratifications than symmetric instabilities.

As $R_o \longrightarrow 1$ for fixed $R_i \in [0.3, 40]$, nonhydrostatic terms become more important. Stone (1971) observed that Dw/Dt always decreases growth rates for both instabilities and his result is verified by the thin contours of figures 5 and 6. In our extension of

Stone's analysis, we find the new result that Dw/Dt together with Coriolis terms from the meridional component of rotation initially enhance instability growth rates before decreasing which is indicated by a bulge in the thick contours of the same figures.

Instability growth rate curves also provide information about critical wavenumbers and, consequently, length scale. For the baroclinic instability, growth rate curves versus wavenumber have a definite peak, and modes with highest growth rates will dominate the instability evolution. Thus, the critical wavenumber, k_c, is the wavenumber at peak growth rate. As observed in the previous section, inclusion of tilted rotation in a nonhydrostatic model makes only minor modifications to k_c at intermediate values of R_o.

For the symmetric instability, growth rates increase sharply with λ beginning at some minimum value then level at maximum by $\lambda \approx 50$. Inclusion of Dw/Dt and $\cot\phi_o$ does not alter this behavior, and choosing the wavelength of maximum growth does not provide new information. However, what is new is that the minimum wavenumber, i.e. largest scale, at which the instability occurs is modified by tilted rotation (figure 4), and we can capture this behavior by choosing the minimum wavenumber as λ_c. In any case, we are interested in trends in the horizontal length scale of the instability as modified by full nonhydrostatic effects and remark that one needs to be cautious before extrapolating conclusions about length scale from a linear stability prediction to the full nonlinear stability problem.

The contours of figure 7 were derived by converting λ_c into the critical wavelength, $L_c = 2\pi D R_o \lambda_c^{-1}$, and normalizing by the ocean depth, D. Thick lines are contours for which Dw/Dt and tilted rotation are included, while thin lines were evaluated from the traditional nonhydrostatic model. Regimes of negative q (marked "unstable") are bounded by the dotted vertical line at $R_i = 1$, valid for the hydrostatic and traditional nonhydrostatic models, and the thick dash-dotted line defined by (2.16) and appropriate

for the nonhydrostatic equations with tilted rotation. Clearly, decreasing R_o at fixed R_i, corresponds to decreasing horizontal length scale and, as previously stated, increasing the relative importance of nonhydrostatic terms. The reduction in scale of symmetric instabilities with decreasing R_o is not as pronounced in the fully nonhydrostatic model. For example, at $R_i = 0.9$ and stratifications typical of LS and SO, the hydrostatic and traditional nonhydrostatic models predict a horizontal wavelength of D and $3D$, respectively, while the nonhydrostatic model with tilted rotation predicts $3D$ and $6D$, respectively.

If we interpret L_c/D as the inverse aspect ratio, δ^{-1}, and note that $R_o = \delta^{-1}U/(f_o L_c) \equiv \delta^{-1}R_o^*$, where we have used the notation superscript $*$ to differentiate the Rossby number (R_o^*) from the baroclinicity (thermal Rossby number, R_o), then we obtain figure 8. Each solid ($Dw/dt \neq 0$ and $\cot\phi_o \neq 0$) and dashed ($Dw/Dt \neq 0$ and $\cot\phi_o = 0$) curve in figure 8 represents the evolution of an unstable mode in the space of δ and R_o^* at constant R_i as the baroclinicity, R_o, changes. Lines increase in thickness with increasing R_i. Small R_o solutions for the full equations collapse to a line at $\delta \sim \mathcal{O}(1)$ and $R_o^* \sim \mathcal{O}(0.1)$. In the hydrostatic limit, fixed R_i corresponds to fixed R_o^* and increasing R_o to decreasing δ. That is, the instability time scale is fixed by the R_o^* (R_i) while the "nonhydrostatic" parameter determines the relative scale of horizontal to vertical features. In a hydrostatic model, or, in the case of symmetric modes, a nonhydrostatic model without tilted rotation, instabilities retain these dependencies for all R_o described. This is not the case in a full nonhydrostatic model. The vertical Coriolis (for positive U_z), at small R_o, acts to effectively weaken N changing the stratification time scale and the Rossby number. As R_i approaches and exceeds 1, the remaining symmetric modes are fundamentally nonhydrostatic, vanishing with increasing baroclinicity. The dash-dotted line, included in the

plot for a reference, has a -1 slope which parallels the $R_i = 1$ line and the collapsed modes at small R_o. At higher R_i, changes in baroclinicity primarily alter R_o^* and not δ.

3.1. *Energetics*

In the previous sections, we have demonstrated that a tilted rotation axis in a nonhydrostatic model expands the unstable regime of the symmetric instability and decreases the dominance regime of the baroclinic instability. We have also demonstrated an R_o dependence in horizontal length scale for symmetric instabilities and growth rates for both types of shear instabilities. However, it remains unclear if and how these features modify the driving mechanisms of the instabilities and whether an R_o dependence is evident in mean to eddy energy production and conversion rates.

In general, dependent variables, η, have a mean and fluctuating component, i.e. $\eta = \overline{\eta} + \eta'$, where we define zonal (mean) averages by

$$\overline{\eta} = \frac{1}{L}\int_{-L/2}^{L/2} \eta dx \tag{3.1}$$

An equation for the production rate of zonal mean kinetic energy, $K_M = \overline{\mathbf{u}} \cdot \overline{\mathbf{u}}/2$, is found by taking the dot product of the averaged momentum equation (2.2):

$$\begin{aligned}
\frac{\overline{D}K_M}{Dt} &= -\overline{u_k}\partial_j\overline{u_j'u_k'} - \overline{v}\Theta_y - \overline{w}\Theta_z + \overline{w}B \\
&= -\boldsymbol{\nabla}\cdot(\overline{\mathbf{u}'u_k'}\overline{u_k}) + \overline{\mathbf{u}'u_k'}\cdot\boldsymbol{\nabla}\overline{u_k} - \boldsymbol{\nabla}\cdot\overline{\mathbf{u}}\Theta + \overline{w}B \\
&= -\boldsymbol{\nabla}\cdot(\overline{\mathbf{u}'u'}z) + \overline{u'w'}
\end{aligned} \tag{3.2}$$

where $\overline{D}/Dt = \partial/\partial t + \overline{\mathbf{u}}\cdot\boldsymbol{\nabla}$ and subscripts i, j, k correspond to x, y, z components, respectively. The equation for the zonally averaged eddy kinetic energy, $K_E = [(u')^2 + (v')^2 + Ro^{-2}(w')^2]/2$, is similarly derived from the momentum perturbation equations (2.9). Taking $\mathbf{u}' \cdot D\mathbf{u}'/Dt$ and averaging:

$$\frac{\partial K_E}{\partial t} = -\overline{u_k' \mathbf{u}'} \cdot \nabla \overline{u_k} - \nabla \cdot \overline{\mathbf{u}'\theta'} + \overline{b'w'}$$
$$= -\overline{u'w'} - \nabla \cdot \overline{\mathbf{u}'\theta'} + \overline{b'w'} \tag{3.3}$$

The equation for the production rate of eddy potential energy, $P_E = \overline{b'b'}/(2B_z)$, is found by multiplying the perturbation buoyancy equation by b' and averaging:

$$\frac{\partial P_E}{\partial t} = -\frac{\overline{b'\mathbf{u}'} \cdot \nabla B}{B_z} = -\overline{b'w'} - \overline{b'v'}\frac{B_y}{B_z} \tag{3.4}$$

Finally, zonal mean available potential energy $P_M = \overline{P} - P_E$ where $\overline{P} = -zB$ is

$$\frac{\overline{D} P_M}{Dt} = \nabla \cdot (z\overline{\mathbf{u}'b'}) + \overline{b'v'}\frac{B_y}{B_z} \tag{3.5}$$

(3.2)–(3.5) together with the linear approximations to the perturbation variables evaluated in section 2 provide a second order estimate of the production/loss rate of the base state and eddy energies. From the above equations, we define the conversion rates $C(A \rightarrow B)$ where $A \rightarrow B$ indicates a direct transfer of energy from source A to source B at the rate C:

$$C(K_E \rightarrow K_M) = \overline{u'w'}$$
$$C(P_E \rightarrow K_E) = \overline{b'w'}$$
$$C(P_M \rightarrow P_E) = -\overline{b'v'}\frac{B_y}{B_z}$$
$$C(K_M \rightarrow P_M) = 0 \tag{3.6}$$

while the fluxes are defined as

$$F(K_E) = \overline{\mathbf{u}'\theta'}$$
$$F(P_E) = 0$$

$$F(K_M) = z\overline{\mathbf{u}'u'}$$

$$F(P_M) = -z\overline{\mathbf{u}'b'}. \tag{3.7}$$

3.2. *Globally Averaged Conversions and Production Rates*

Modes tending to symmetric instability have y and z dependencies and a zonal average is trivially defined $\overline{u'v'} = 2\pi k^{-1}u'v'$. For each baroclinic mode, we have $u' = \mathrm{Re}\{\check{u}(z,t)\exp(ikx)\}$ and $v' = \mathrm{Re}\{\check{v}(z,t)\exp(ikx)\}$, and a zonal average may be defined by

$$\begin{aligned}\overline{u'v'} &= \int_0^{2\pi/k} \mathrm{Re}\{\check{u}\exp(ikx)\}\mathrm{Re}\{\check{v}\exp(ikx)\}dx = \frac{\pi}{k}\mathrm{Re}\{\check{u}\check{v}^*\} \\ &= \frac{\pi}{k}\exp(2\sigma_i t)\mathrm{Re}\{\hat{u}(z)[i\hat{v}(z)]^*\}\end{aligned} \tag{3.8}$$

where $\sigma_i = -\mathrm{Im}(\sigma)$. However, in both cases the global average is simply

$$< \overline{u'v'} > = \frac{\lambda k}{2\pi^2}\exp(-2\sigma_i t)\int_0^1 \int_{-\pi/\lambda}^{\pi/\lambda} \overline{u'v'}dydz = \int_0^1 \mathrm{Re}\{\hat{u}[i\hat{v}]^*\}dz. \tag{3.9}$$

Unstable modes have three nonzero conversion rates, globally integrated:

$$\begin{aligned}< C(K_E \rightarrow K_M) > &= < \overline{w'u'} > \\ < C(P_E \rightarrow K_E) > &= < \overline{w'b'} > \\ < C(P_M \rightarrow P_E) > &= \frac{< \overline{v'b'} >}{R_i - R_o^{-1}\cot\phi_o}\end{aligned} \tag{3.10}$$

The globally integrated fluxes for rigid top and bottom boundaries are zero.

For baroclinic instabilities, the positive $< C(P_M \rightarrow P_E) > \equiv C_o$ continues to be the highest conversion rate regardless of baroclinicity (Stone (1972)) and R_i. Tilted rotation increases the relative rate $C_o^{-1} < C(P_E \rightarrow K_E) >$ by only about 5% compared to the traditional nonhydrostatic result under conditions of small N (LS) where these effects are most prominent. In general, the "traditional" baroclinic energy cycle, $P_M \longrightarrow P_E \rightarrow K_E$,

applies equally well to hydrostatic and nonhydrostatic models with or without tilted rotation.

Symmetric instabilities are, however, nonhydrostatic for a much larger range of R_o than baroclinic instabilities, and the modifications due to tilted rotation are more pronounced and challenge the traditional interpretation of the energy cycle. In the hydrostatic limit, global energy conversions are dominated by $< C(K_E \rightarrow K_M) > \equiv -C_o < 0$. That is, base kinetic energy is the primary source driving the production of eddy kinetic energy for the symmetric instability (Eliassen and Kleinschmidt (1957)).

Total energy production rates normalized by C_o are plotted in figure 9 versus R_o for (a) $R_i = 0.9$ and (b) $R_i = 0.5$. Thick lines were derived from the nonhydrostatic model with tilted rotation, while thin lines are results which include Dw/Dt but assume a vertical rotation axis. Mean kinetic (horizontal dotted line) and mean potential rates (solid lines) are negative, i.e. losses, which is expected as the base state drives the instability. The eddy production rates are indicated by dashed lines for the eddy potential energy and dash-dotted lines for the eddy kinetic energy. Vertical dotted lines mark values of R_o consistent with constant N typical of LS, SO and BB.

The energy production rates for both nonhydrostatic models become independent of R_o and, thus, equivalent to the hydrostatic result, at base N near that of BB. In this limit, the magnitude of K_M loss rates exceed that of P_M by an order of magnitude. In nonhydrostatic solutions with tilted rotation, the relative conversion $C_o^{-1} < C(P_M \rightarrow P_E) >$ begins to play a larger role for $R_o \leqslant$ that of SO. For both nonhydrostatic models we see an increased role for the P_M in driving the instability, however, without tilted rotation DP_M/Dt remains secondary to DK_M/Dt in our oceanic parameter range. From figure 9 this is not the case when full nonhydrostatic effects are included. At values of R_o in the vicinity of LS, $|DP_M/Dt|$ exceeds $|DK_M/Dt|$ and P_M becomes the dominant

energy source for the instability. This transition coincides with a sharp relative increase in P_E production not evident in the traditional nonhydrostatic results.

4. Conclusions

In this work, we have extended Stone's pioneering study of the symmetric and baroclinic instabilities to include a non-vertical axis of rotation. From a linear stability analysis, we have shown that tilted rotation modifies the base state fields from the traditional nonhydrostatic model in two ways: 1) increasing the absolute momentum vertical gradients and 2) decreasing the modified buoyancy vertical gradients. Both modifications decrease base Ertel potential vorticity (q), push the symmetric boundary of existence to larger R_i's, and, thus, impact dominance regimes for symmetric and baroclinic instabilities. Since growth rates for symmetric instabilities are about a factor of 5 greater than baroclinic rates in regions of negative q, except in a small neighborhood of the boundary, a nonzero meridional rotation component together with a positive zonal z-shear enhances the symmetric dominance regime at the expense of the baroclinic regime. In regions of weak stratification like the Labrador Sea, symmetric growth rates exceed that of baroclinic modes for R_i of almost 2, whereas the traditional nonhydrostatic result predicts a transition to baroclinic dominance at $R_i = 0.95$.

Our work is consistent with and supports that of Hathaway et al. (1979), Sun (1994) and Mu et al. (1998) who include tilted rotation in their analyzes of the symmetric instability but do not decouple the static stratification from the vertical Coriolis and, therefore, do not explore the effects of modifications to the vertical gradients of the buoyancy field.

Contrary to the conclusions of Stone (1971), growth rates for symmetric and baroclinic instabilities at fixed latitude and R_i are not maximal in the hydrostatic limit. Rather,

growth rates peak at intermediate values $R_o \sim \mathcal{O}(1)$ in the nonhydrostatic equations with tilted rotation. This is also the regime for which deviations from the hydrostatic result are most important, since at very small R_o, deviations from hydrostatic may be large, but growth rates are negligible. Significantly, the $\mathcal{O}(1)$ parameter regime is physically relevant and consistent with oceanic measurements of stratifications in the Labrador Sea and Southern Ocean for $R_i < 20$.

Symmetric instabilities are confined to smaller horizontal scales than baroclinic instabilities, and these scales are bounded by some maximum wavelength which varies with R_o. Tilted rotation maintains these instabilities to larger horizontal scales, i.e. greater maximum wavelengths, which is potentially important for global scale numerical modelling and regional numerical models which resolve scales approximately an order of magnitude smaller than that of baroclinic instabilities. For baroclinic instabilities, estimates of length scale changes due to the hydrostatic and traditional approximations are minor. Our present stability analysis provides useful information about trends and relative length scales but not accurate estimates which depend on nonlinear effects. In future work, we will investigate the role of tilted rotation and its impact on spatial scale in a nonlinear numerical model of the 3D nonhydrostatic Boussinesq equations.

We have also applied our results to parameter regimes relevant to the physical ocean. Stratification is identified as an important parameter in assessing a region's sensitivity to nonhydrostatic effects, at least in our limited latitude range (30^o to 60^o). The weak stratifications of the Southern Ocean, the Labrador Sea and high-latitudes in general make these regions most sensitive to the nonhydrostatic effects described in this work. We suggest that implementation of the fully nonhydrostatic equations should be considered for high-latitude numerical modelling.

Finally, we have shown that tilted rotation modifies the energy cycle of symmetric

instabilities. Our analysis compares relative changes in the energy conversion rates between base and eddy flow and total energy production/loss rates. The hydrostatic picture of symmetric eddy rolls driven by base state kinetic energy is not accurate in parameter regimes appropriate for the Labrador Sea where tilted rotation and nonhydrostatic effects are important. Rather, the base state potential energy, the primary source in baroclinic instabilities, contributes comparably potentially exceeding that of base state kinetic energy in driving symmetric eddies.

REFERENCES

Eady, E. T., 1949: Long waves and cyclone waves. *Tellus*, **1**, 33–52.

Eliassen, A. and E. Kleinschmidt, 1957: *Handbuch der Physik, vol. 48*. Springer-Verlag, 154 pp.

Hathaway, D. H., P. A. Gilman, and J. Toomre, 1979: Convective instability when the temperature gradient and rotation vector are oblique to gravity 1. fluids without diffusion. *Geophys. Astrophys. Fluid Dynamics*, **13**, 289–316.

Heywood, K. J., A. N. Garabato, and D. P. Stevens, 2002: High mixing rates in the abyssal southern ocean. *Nature*, **415**, 1011–1014.

Hoskins, B. J., 1978: Baroclinic instability. *Rotating Fluids in Geophysics*, P. H. Roberts and A. M. Soward, eds., Academic Press, 171–203.

Lasier, J. R. N., 1980: Oceanographic conditions at o. w. s. bravo 1964–1974. *Atmos.-Ocean*, **18**, 227–238.

Mu, M., V. Vladimirov, and Y. Wu, 1998: Energy-casimir and energy-lagrange methods in the study of nonlinear symmetric stability problems. *J. Atmos. Sci.*, **56**, 400–411.

Ooyama, K., 1965: On the stability of the baroclinic circular vortex: a sufficient criterion for instability. *J. Atmos. Sci.*, **23**, 43–53.

Stone, P. H., 1966: On non-geostrophic baroclinic stability. *J. Atmos. Sci.*, **23**, 390–400.

— 1971: Baroclinic stability under non-hydrostatic conditions. *J. Fluid Mech.*, **45**, 659–671.

--- 1972: On non-geostrophic baroclinic stability: Part iii. the momentum and heat transports. *J. Atmos. Sci.*, **29**, 419–426.

Straneo, F., M. Kawase, and S. C. Riser, 2000: Idealized models of slantwise convection in a baroclinic flow. *J. Phys. Oceanogr.*, **32**, 558–572.

Sun, W.-Y., 1994: Unsymmetrical symmetric instability. *Q. J. R. Meteorol. Soc.*, **121**, 419–431.

van Aken, H. M., H. van Haren, and L. R. M. Maas, 2007: The high-resolution vertical structure of internal tides and near-inertial waves measured with an adcp over the continental slope in the bay of biscay. *Deep-Sea Res. I*, **54**, 533–556.

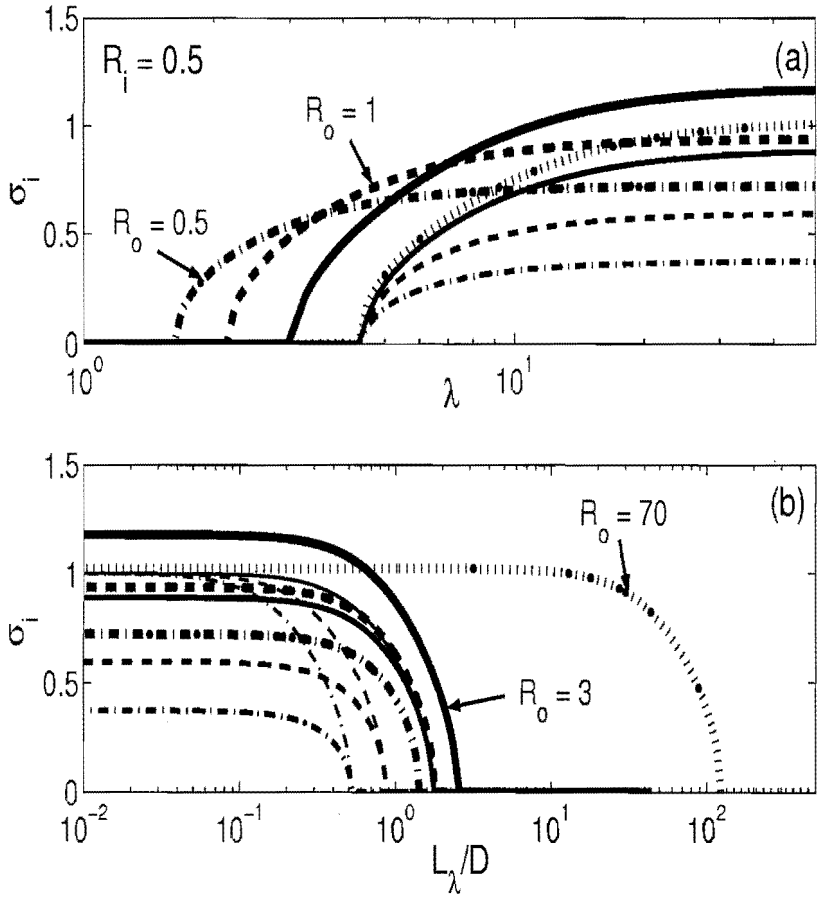

FIGURE 1. A comparison of growth rates for the symmetric instability between the fully nonhydrostatic model (thick lines), Stone (1971)'s fig. 2 nonhydrostatic results with $F = 0$ (thin lines), and the hydrostatic results (thinnest lines in (b) only). In (a), growth rates for four baroclinicities are plotted versus the non-dimensional wavenumber (λ) which in dimensional units scales with R_o. We have added an intermediary value of the baroclinicity, $R_o = 3$, for comparison to highlight a novel feature of the nonhydrostatic model with tilted rotation: symmetric growth rates do not peak in the hydrostatic limit but, rather, at values of $R_o \sim \mathcal{O}(1)$. In (a), all hydrostatic lines converge with the $R_o = 70$ (dotted) nonhydrostatic solutions. In (b), growth rates for the same four baroclinicities are plotted against wavelength, $L_\lambda/D = 2\pi R_o \lambda^{-1}$, normalized by the vertical depth to remove the implicit R_o dependence and clarify the scale dependence. When tilted rotation is included in a nonhydrostatic model, the cut-off maximum meridional wavelength of the symmetric instability moves to larger scales. Maximum wavelengths of the traditional nonhydrostatic and hydrostatic solutions are identical. Latitude is fixed at 45°.

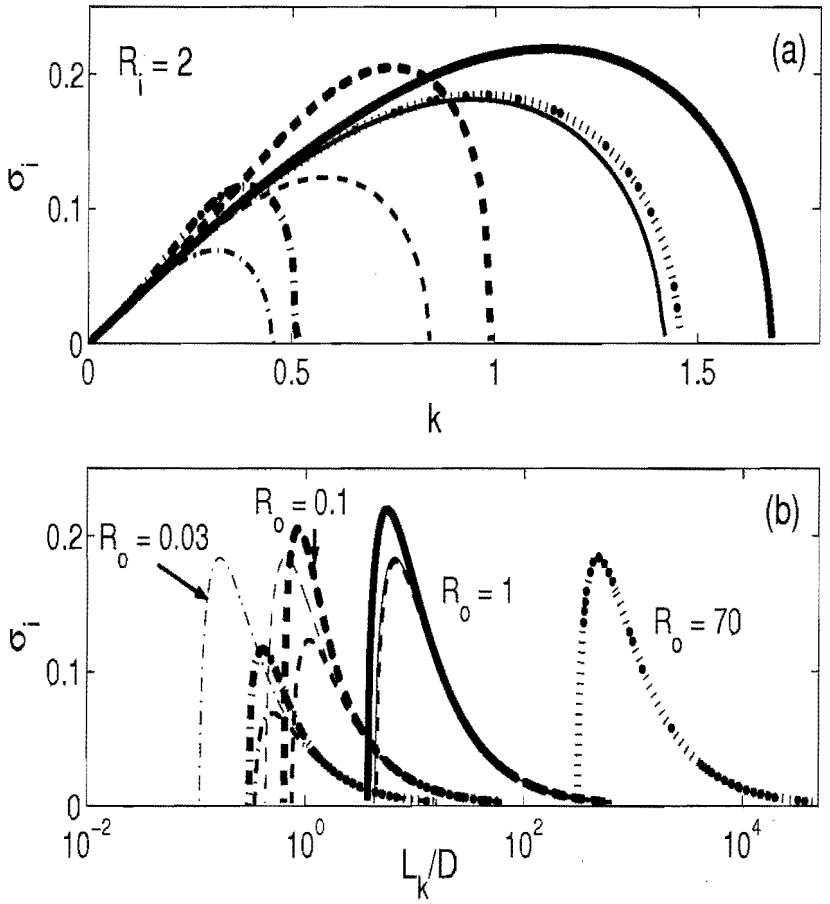

FIGURE 2. A comparison of baroclinic growth rates from (2.18) which include nonhydrostatic effects and tilted rotation (thick lines) and Stone (1971)'s fig. 1 which includes Dw/Dt but assumes $F = 0$ (thin lines) with $R_o = 70$ (dotted), 0.1 (dashed), and 0.03 (dash-dotted). We have added $R_o = 1$ (solid) to illustrate two novel features of the nonhydrostatic equations with tilted rotation: 1) baroclinic growth is most sensitive to values of $R_o \sim \mathcal{O}(1)$ where rates become maximal, and 2) as R_o decreases from the hydrostatic limit at fixed R_i, growth rates initially increase exceeding that of the hydrostatic model. Since the wavenumber k scales with R_o, we have also plotted, in (b), growth rates versus wavelength, $L_k/D = 2\pi R_o k^{-1}$, normalized by the vertical depth. Thinnest lines, evident in (b) only, are solutions of the hydrostatic model. In (a), all hydrostatic lines converge to the $R_o = 70$ (dotted line). Latitude is 45°.

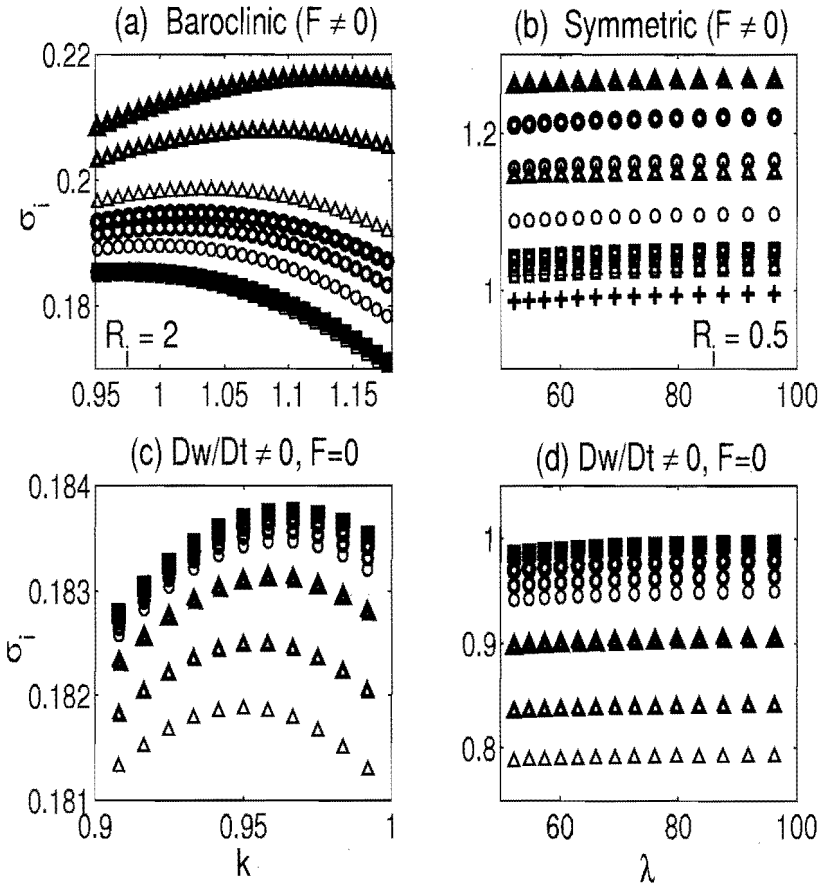

FIGURE 3. Baroclinic ($R_i = 2$ (a) and (c)) and symmetric ($R_i = 0.5$ (b) and (d)) growth rates versus wavenumbers for a range of latitudes (in order of decreasing thickness): $\phi_o = 30°$, 45°, and 60°; and stratifications typical of the following locations: Labrador Sea (△), Southern Ocean (o), and Bay of Biscay (□). The hydrostatic results in (a)–(d) are indicated by + (visible in (b) only) and are coincident with the filled □ of the BB growth rate curves for (a), (c), and (d). Upper plots ((a) and (b)) are from nonhydrostatic equations with tilted rotation, while lower plots ((c) and (d)) are from the traditional nonhydrostatic equations which include Dw/Dt but assume strictly vertical rotation. For the baroclinic plots on the left, changes in stratification account for greater variations in non-dimensional growth rates than occur for changes in latitude. For both instabilities, the regions most sensitive to tilted rotation and Dw/Dt are those with weak static stratifications even at latitudes of 60°.

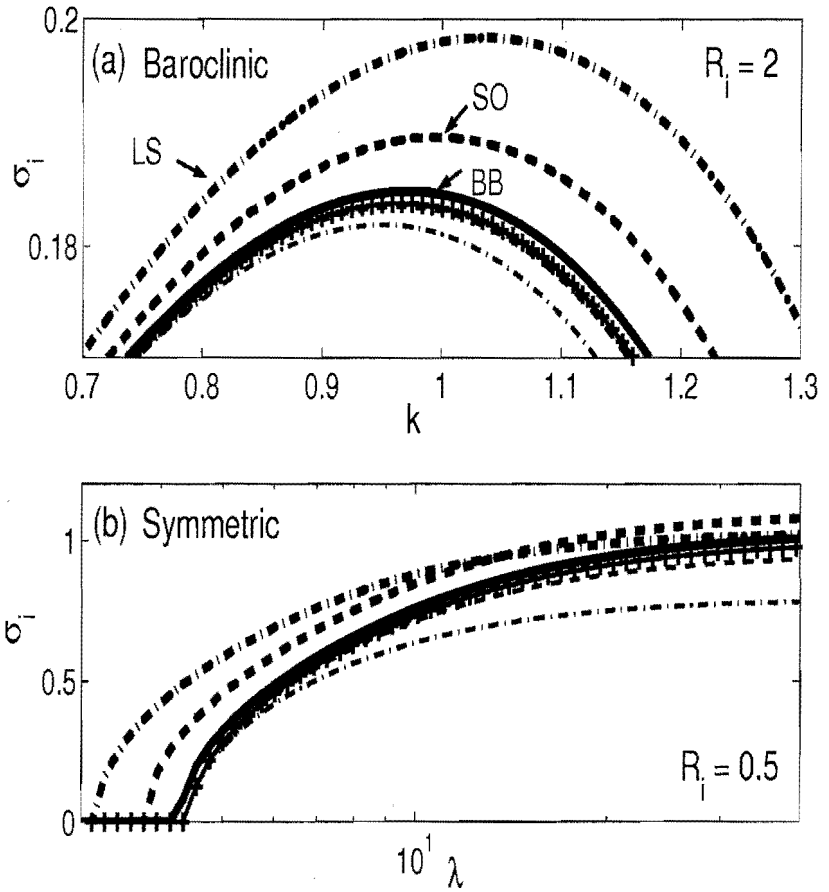

FIGURE 4. (a) Baroclinic ($R_i = 2$) and (b) symmetric ($R_i = 0.5$) growth rates at 60° latitude with stratifications typical of the following locations: Labrador Sea (dash-dot), Southern Ocean (dash), and Bay of Biscay (solid). Baroclinicities for the regions are as follows: BB (in (a) $R_o = 20$ and (b) $R_o = 30$)), SO (in (a) $R_o = 3$ and (b) $R_o = 6$), and LS (in (a) $R_o = 1$ and (b) $R_o = 2$). Thick lines include tilted rotation and Dw/Dt, while thin lines include Dw/Dt but assume a locally vertical rotation vector. The hydrostatic result is indicated by +. Inclusion of full nonhydrostatic terms increases growth rates for all three regions though at high-latitude the effect is less pronounced than shown in figures 1 and 2 at $\phi_o = 45°$. The key baroclinicities, $R_o \sim \mathcal{O}(1)$, for which enhancement of growth rates due to nonhydrostatic terms is most significant, are physically relevant and well characterized by the above three oceanic regions.

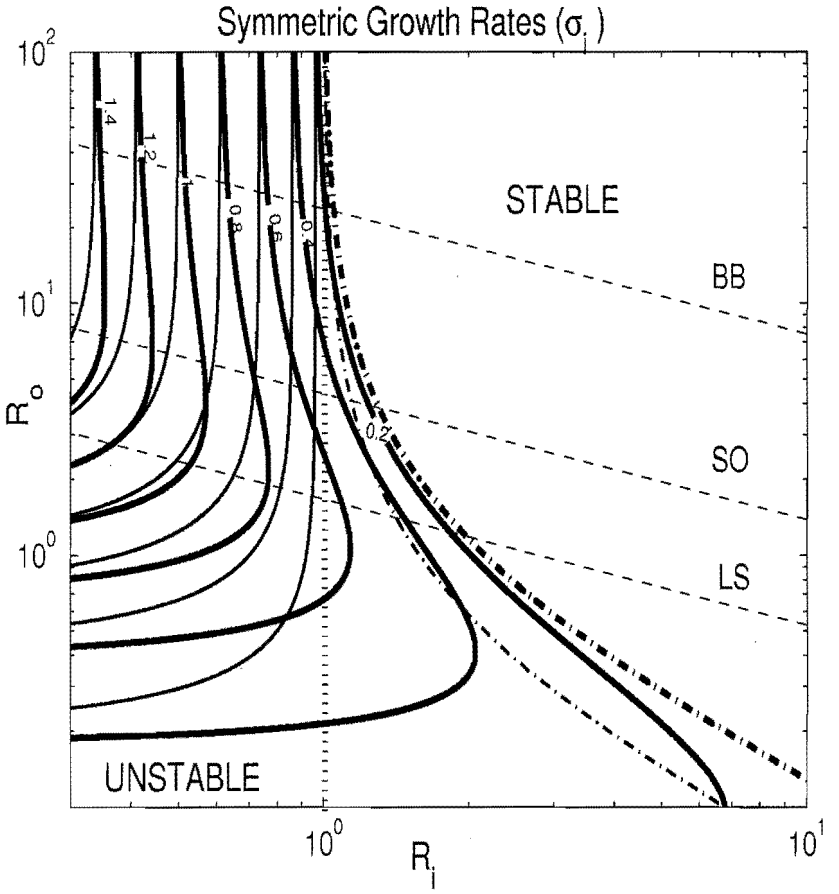

FIGURE 5. Contours of maximum growth rate for the symmetric instability at $\phi_o = 60°$. Thick solid lines are solutions which include tilted rotation and Dw/Dt, and thin solid lines are from traditional nonhydrostatic equations ($Dw/Dt \neq 0$ and $\cot\phi_o = 0$). Dashed lines are of constant N typical of the Bay of Biscay (BB), Southern Ocean (SO) and Labrador Sea (LS). The dotted line at $R_i = 1$ marks the boundary for existence of the symmetric instability according to Stone (1971)'s necessary condition when $\cot\phi_o = 0$, the thick dash-dotted line defines the existence boundary according to (2.16), and the thin dash-dotted line marks the instability criteria of Sun (1994). Symmetric maximum growth rates *exceed* maximum baroclinic rates in regions of negative q except in a small neighborhood of the boundary. This boundary, for LS, reaches $R_i \approx 2$ with tilted rotation and Dw/Dt, nearly double that of the traditional nonhydrostatic and hydrostatic results.

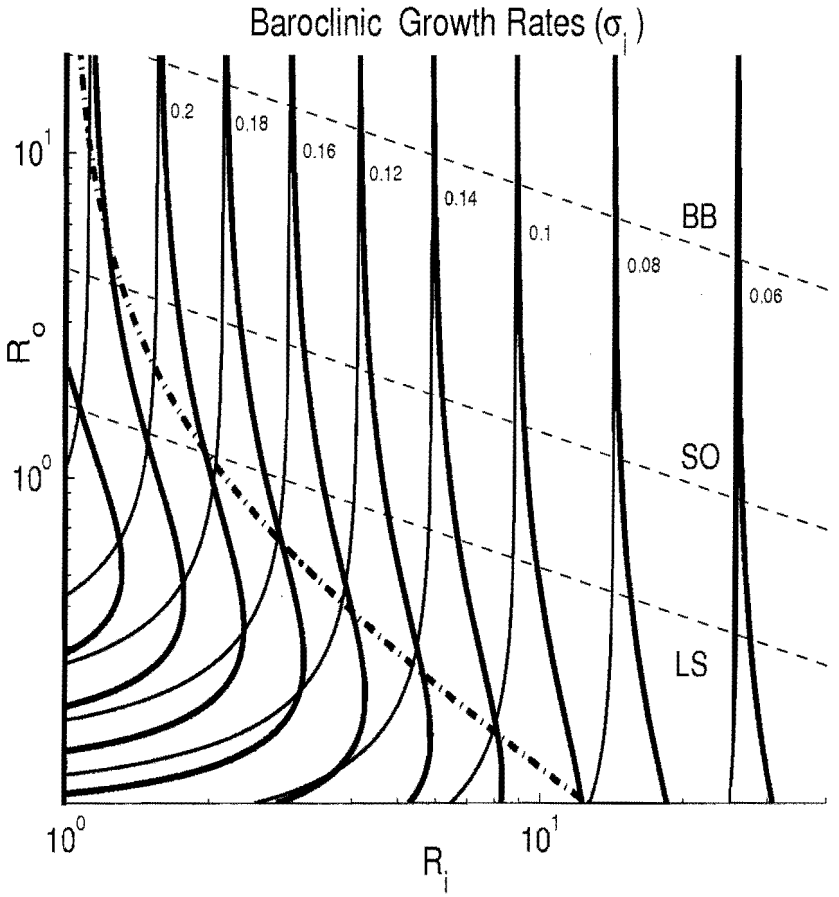

FIGURE 6. Contours of maximum growth rate for the baroclinic instability at $\phi_o = 60^o$. Thick solid lines are solutions which include tilted rotation and Dw/Dt, and thin solid lines are from traditional nonhydrostatic equations ($Dw/Dt \neq 0$ and $\cot\phi_o = 0$). Dashed lines are of constant N typical of the Bay of Biscay (BB), Southern Ocean (SO) and Labrador Sea (LS). Regimes of negative q, for which the symmetric instability occurs and dominates except very near the boundary, are indicated by the parameter space to the left of the thick dash-dotted line, when full nonhydrostatic effects are included, and by the vertical axis $R_i = 1$, when either a hydrostatic model or Stone (1971)'s traditional nonhydrostatic model is assumed. Inclusion of tilted rotation in the nonhydrostatic model reduces the parameter space for which baroclinic instabilities dominate, and this effect is most pronounced for stratifications typical of the high-latitude regions. For further details see figure 5

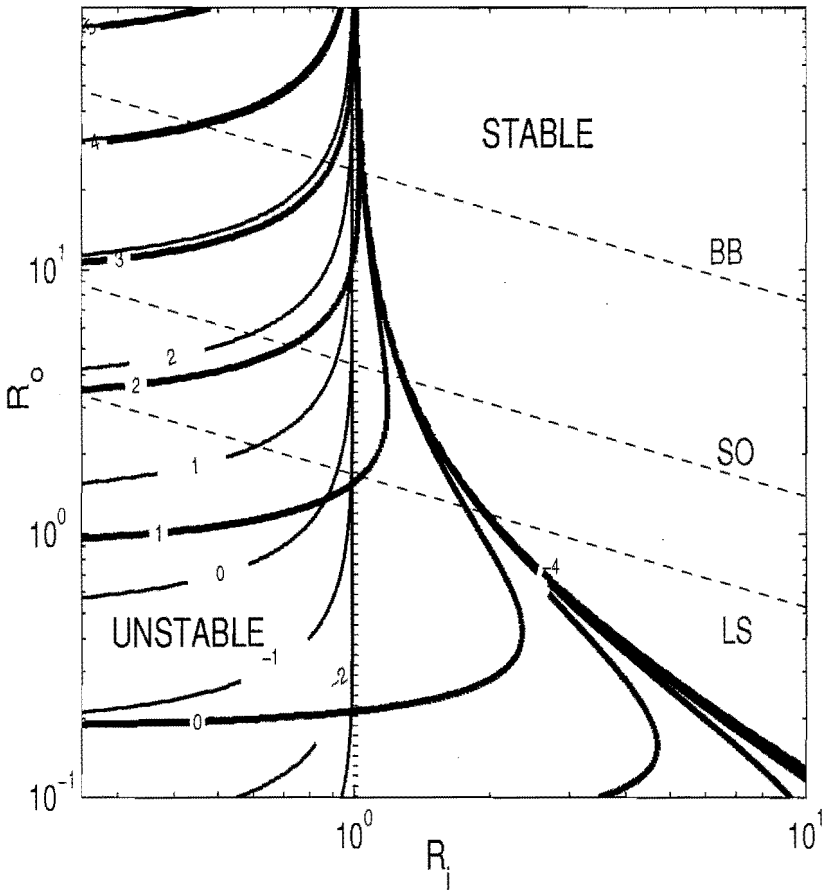

FIGURE 7. Contours of $\log(L_c/D)$ (largest wavelength, $2\pi R_o \lambda_c^{-1}$, for which solutions have unstable growth rates), in the parameter space of R_i and R_o. Thick lines include nonhydrostatic effects with tilted rotation, and thin lines include Dw/Dt as in Stone (1971) but with $F = 0$ and are identical to the hydrostatic result. Dashed lines mark constant N typical of LS (Labrador Sea), SO (Southern Ocean) and BB (Bay of Biscay). Regimes of negative q (marked "unstable") are bounded by the dotted line at $R_i = 1$ obtained from Stone (1971)'s necessary condition for instability when $F = 0$ and the thick dash-dotted line obtained from the existence criteria of (2.16). Decreasing R_o at fixed R_i increases the relative importance of nonhydrostatic terms and decreases the largest horizontal scale of the instability for all models plotted. However, this reduction in scale is less pronounced in the fully nonhydrostatic model, and maximum length scales are double and triple that of the hydrostatic model for SO and LS near $R_i = 1$.

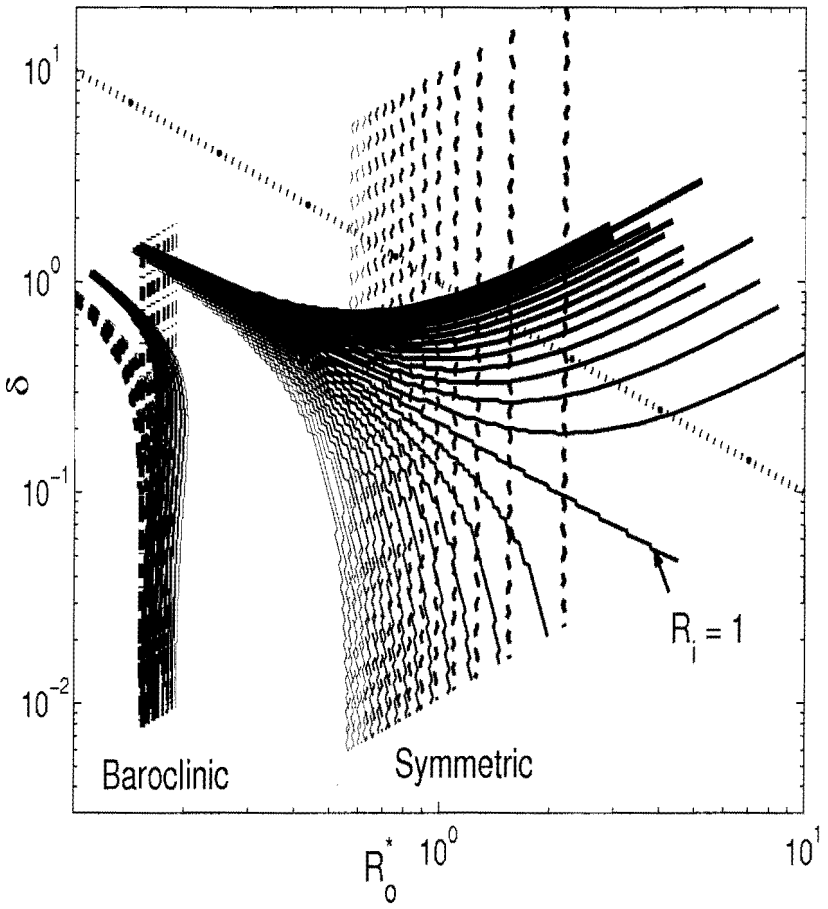

FIGURE 8. Lines of constant R_i at $\phi = 60^\circ$ in the space of aspect ratio, $\delta = D/L_c$, and Rossby number, $R_o^* = U/(f_o L_c)$, where for the symmetric perturbations, $L_c = 2\pi D R_o \lambda_c^{-1}$ is the largest wavelength unstable to symmetric rolls and for the baroclinic instability, $L_c = 2\pi D R_o k_c^{-1}$ is the wavelength of maximum baroclinic growth rates. For both instabilities, lines increase in thickness with increasing R_i. Dashed lines are from solutions of the traditional nonhydrostatic equations: 1) for symmetric, $R_i = [0.25, 0.99]$ and 2) for baroclinic, $R_i \in [1, 2]$. In the case of symmetric modes, the vertical lines also align with the hydrostatic modes which indicates that increasing/decreasing R_o for solutions without tilted rotation corresponds directly to decreasing/increasing δ. Hydrostatic baroclinic modes (dash-dotted lines) are also vertical at constant R_i and the previous conclusion holds. This is not the case in the fully nonhydrostatic model. Solid lines include both tilted rotation and Dw/Dt: 1) for symmetric, $R_i \in [0.25, 1.7]$ and 2) for baroclinic, $R_i \in [1, 2]$. Although these modes converge with the hydrostatic for large R_o (small δ), at small R_o, modes collapse to a line at $\delta \sim \mathcal{O}(1)$ and $R_o^* \sim \mathcal{O}(0.1)$. The dotted line is included for reference and slopes with -1. Above $R_i = 1$ (the "traditional" symmetric boundary), the remaining symmetric modes are fundamentally nonhydrostatic. Increasing/decreasing baroclinicity at fixed R_i corresponds primarily to increasing/decreasing R_o^* with minimal changes in δ.

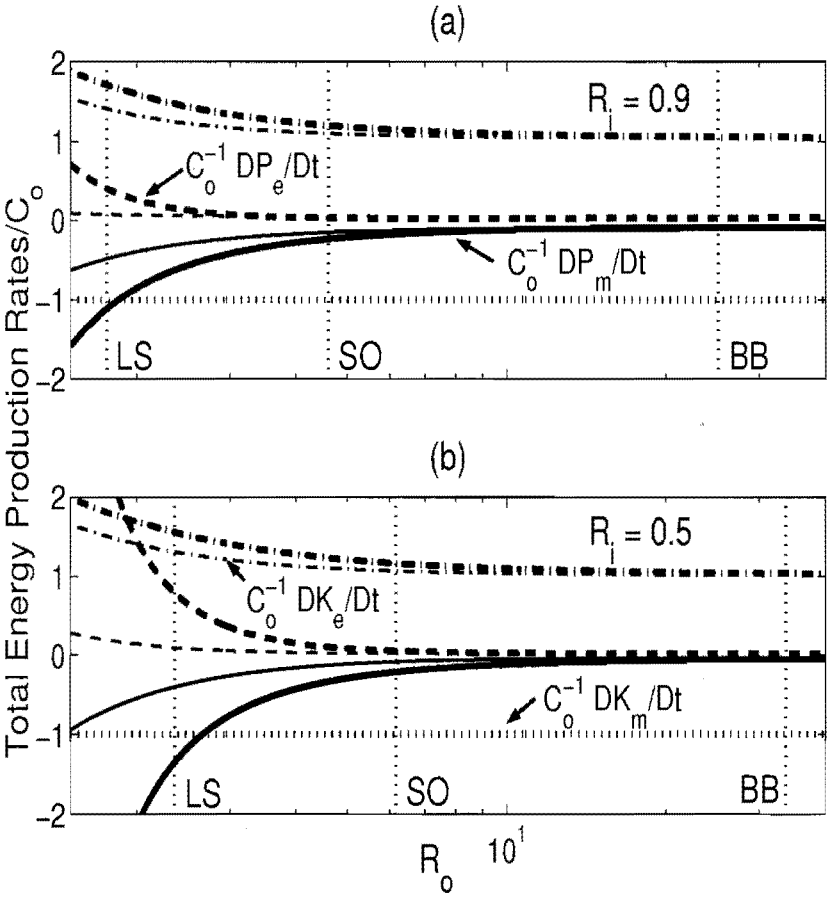

FIGURE 9. Total energy production rates versus baroclinicity for (a) $R_i = 0.9$ and (b) $R_i = 0.5$. Thick lines are from solutions with Dw/Dt and tilted rotation while thin lines are the traditional nonhydrostatic results ($Dw/dt \neq 0$ and $F = 0$). All rates are normalized by $C_o = |C(K_E \rightarrow K_M)|$. Vertical dotted lines indicate constant stratifications typical of LS, SO and BB. Rates for nonhydrostatic models with and without tilted rotation become independent of R_o and, thus, equivalent to the hydrostatic result, at base N near that of BB. As R_o decreases, both models show an increased role for P_M in driving the instability, however, only when tilted rotation is included does $|DP_M/Dt|$ exceeds $|DK_M/Dt|$ for the above physical range of R_o. Latitude is 60°.